INCLUSION NUCLEATION, GROWTH, AND MIXING DURING STEEL DEOXIDATION

Lifeng ZHANG* and Brian G. THOMAS**

* Research Associate, ** Professor
Dept of Mech. Eng., University of Illinois at Urbana-Champaign
140 Mech. Eng. Bldg., 1206 W. Green St., Urbana, IL 61801, USA
Tel: 1-217-333-6919 Fax: 1-217-244-6534
Email: zhang25@uiuc.edu; bgthomas@uiuc.edu

ABSTRACT

A computational model based on classic homogenous nucleation theory, thermodynamic analysis and numerical simulation, has been developed to study steel deoxidation by aluminum in a low carbon aluminum-killed steel ladle. The model calculates the nucleation and time evolution of the alumina inclusion size distribution due to Ostwald ripening, Brownian collision and turbulent collision. Starting with rapid supersaturation with Al_2O_3 "pseudo-molecules", homogeneous nucleation is very fast, occurring mainly between 1μs and 10μs. The stable inclusion nuclei are predicted to be only about 10-20 Å in diameter. The growth of inclusions smaller than 1μm in radii, is mainly controlled by diffusion of pseudo-molecules and Brownian collision, and inclusions in this range tend to be spherical. The growth of inclusions larger than 2μm in radii is mainly controlled by turbulent collisions, and inclusions in this range tend to form clusters which retain minimum feature sizes of 1~2μm. Inclusion size distribution can reach 0.1~1μm at 6s and 0.1~36μm at 100s. Stirring power has a significant effect on the inclusion size distribution. It is recommended to first stir vigorously to encourage the collision of small inclusions into large ones, followed by a "final stir" that slowly recirculates the steel to facilitate their removal into the slag while minimizing the generation of more large inclusions via collisions.

KEY WORDS: Alumina inclusions, Steel deoxidation, Nucleation, Collision, Growth, Removal, Bubble Flotation, Stirring Power

INTRODUCTION

The demand for cleaner steels increases every year. Steel cleanliness depends on the amount, morphology and size distribution of non-metallic inclusions in steel. There is a growing need to understand and predict the fundamental mechanisms of the formation and removal of inclusion particles from steel during deoxidation and refining operations in ladles and other metallurgical vessels. Inclusions arise from many sources, including deoxidation, reoxidation, slag entrapment, chemical reactions, and exogenous inclusions. [1-8] Their origin can be identified from their composition and shape in the final product, which ranges from dendritic alumina (**Fig. 1a** [9]), formed during deoxidation with a high oxygen content, coral structures from Ostwald ripening of dendritic inclusions (**Fig. 1b** [10]), clusters of particles, formed by collisions of small alumina spheres (**Fig. 1c** [11]), and large spheres of complex oxides, from liquid slag entrainment (**Fig. 1d** [8]). Inclusion evolution and removal is affected by diverse complex phenomena, including deoxidant quantity,

1

composition, and morphology, vessel geometry, transport by turbulent flow, interfacial tension, diffusion coefficient, the initial oxygen content, collisions with both bubbles and other particles, reoxidation, temperature, and properties of the slag layer and vessel walls where inclusions may be removed or generated. Shortly after adding deoxidizer, particles nucleate, precipitate, and quickly grow. Inclusion growth can be controlled by diffusion of the deoxidization elements and oxygen [12-17], "Ostwald-ripening"[12, 13, 17-19], Brownian collisions [12-15, 17], turbulent collision [12-14, 18] and Stokes collision [13, 15, 17-19]. With improved computer power, better computational models of these phenomena are being developed.
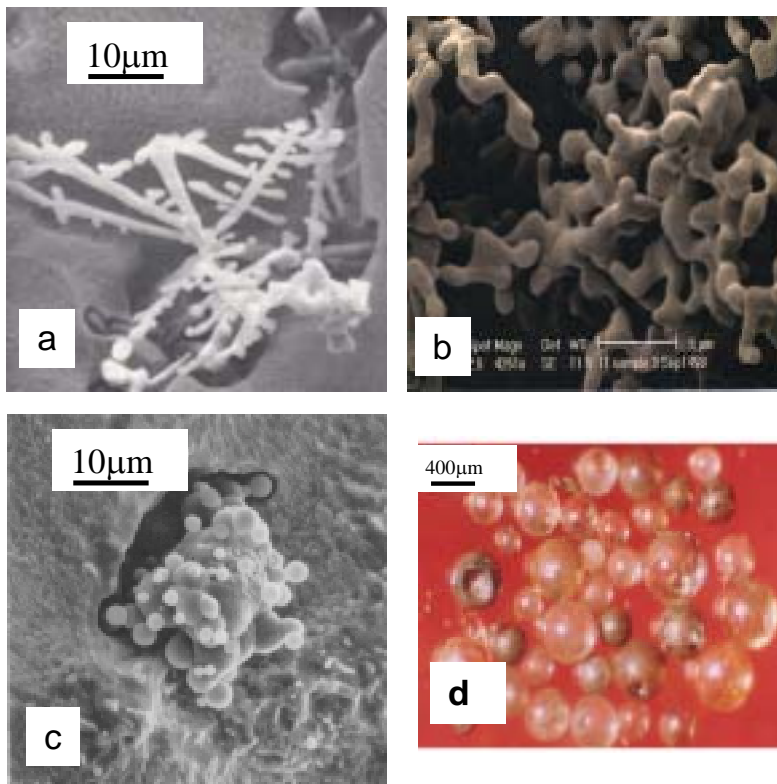

Fig. 1 Alumina inclusion morphologies: a) dendritic cluster [9], b) coral structure [10] c) alumina cluster [11], and d) slag inclusions [8]

This paper presents recent work to simulate the nucleation, growth, transport, and removal of alumina particles during steel deoxidation and discusses the implications on operations such as stirring and refining. A common characteristic of the indigenous alumina inclusions in Low Carbon Al-Killed (LCAK) steel [9-12, 20-29] is that the central globule, secondary dendrite arms, or the individual spherical inclusions in an inclusion cluster is consistently 1~4 μm (**Fig. 2**). The reason for this will be investigated in the current paper. The contribution of different growth mechanism on inclusion growth and the start and evolution of inclusion size distribution are also studied.
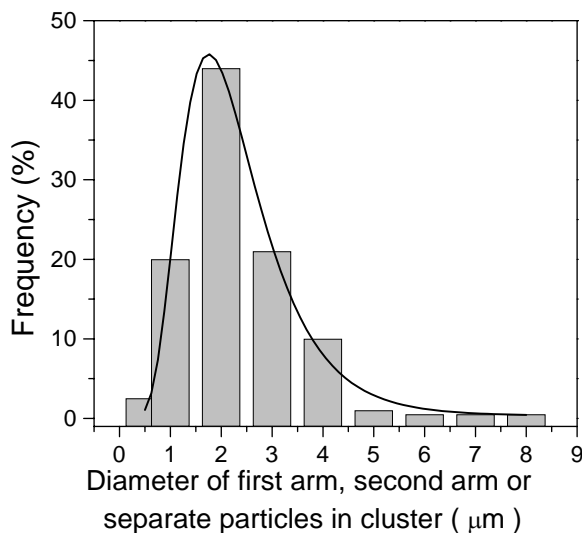

Fig. 2 The smallest size feature of inclusions as shown in Fig.1 a), b) and c).

NUCLEATION AND GROWTH MODELS

The current computational model simulates the nucleation and growth of alumina inclusions during steel deoxidation, starting with a solute of "pseudo-molecules" of Al_2O_3. The assumed time-dependent concentration of pseudo-molecules evolves into a size distribution of molecular groups via diffusion and dissolution. If enough pseudo-molecules gather to form a stable nucleus, then nucleation (precipitation) occurs, meaning that the particle is stable. The stable inclusions can grow both by continued diffusion of pseudo-molecules, and by collision with other nucleated inclusions, via both Brownian and turbulent motion. The following assumptions are included in the model.

① The Gibbs-Thomson equation [30] holds for all size particles; [31]
② The basic unit of the model is the "pseudo-molecule".
③ Ostwald-Ripening is considered, as both diffusion and dissolution of pseudo-molecules are calculated throughout the process.
④ The system is isothermal;
⑤ The pseudo-molecules and clusters (inclusions) are spherical;
⑥ The interfacial tension is independent of particle size.

If the particle size is expressed by the number of Al_2O_3 molecules in the particle, the time evolution of the pseudo-molecules / particles size distribution, N_i, is governed by the following population balance relations:

$2 \leq i < i_C$ (before nucleation)

$$\frac{dN_i}{dt} = -N_i \beta_i^D N_1 + \beta_i^D N_1 N_{i-1} + \alpha_{i+1} A_{i+1} N_{i+1} - \alpha_i A_i N_i \qquad (1)$$

$i \geq i_C$ (after formation of stable inclusion particles)

$$\frac{dN_i}{dt} = \underbrace{-\phi N_i \sum_{j=1}^{\infty} \left(\beta_{ij}^B + \beta_{ij}^T \right) N_j + \frac{1}{2} \phi \sum_{j=1}^{i-1} \left(1 + \delta_{ij} \right) \left(\beta_{j,i-j}^B + \beta_{j,i-j}^T \right) N_j N_{i-j}}_{\textit{Collision of particles causing loss and generation of size i}} \qquad (2)$$

$$\underbrace{- N_i \beta_i^D N_1 + \beta_{i-1}^D N_1 N_{i-1} + \alpha_{i+1} A_{i+1} N_{i+1} - \alpha_i A_i N_i}_{}$$
$$\textit{Diffusion of Molecules to i and dissolution of molecules from i}$$

There are serious computational issues involved in solving Eqs. (1)~(2). These are the computation time and the array limit for memory storage. Because the model is designed to simulate nucleation (concerned with individual molecules with sizes on the order of nanometers) up to collision of real particles (on the order of microns), the particle size range varies over 3 orders of magnitude, containing from 1 to ~10^{13} molecules per particle. Using Eqs. 1 and 2 with a simple linear scale becomes prohibitive for this real system. To make this difficult problem feasible, a simplified model that can accurately handle varying size ranges — Size Group Model — is employed.

SIZE GROUPING MODEL FORMULATION

The concept of this model is shown schematically in **figure 3.** In this model, the inclusions are divided into groups (group number k) with average particle volumes related by the following ratio:

$$\frac{V_k}{V_{k-1}} = R_V \qquad (3)$$

where $2 < R_V < 3$ with 2.5 a typical value. The method can be developed for other choices of R_V, but the following equations change slightly. With this assumption, the radius and the volume of each
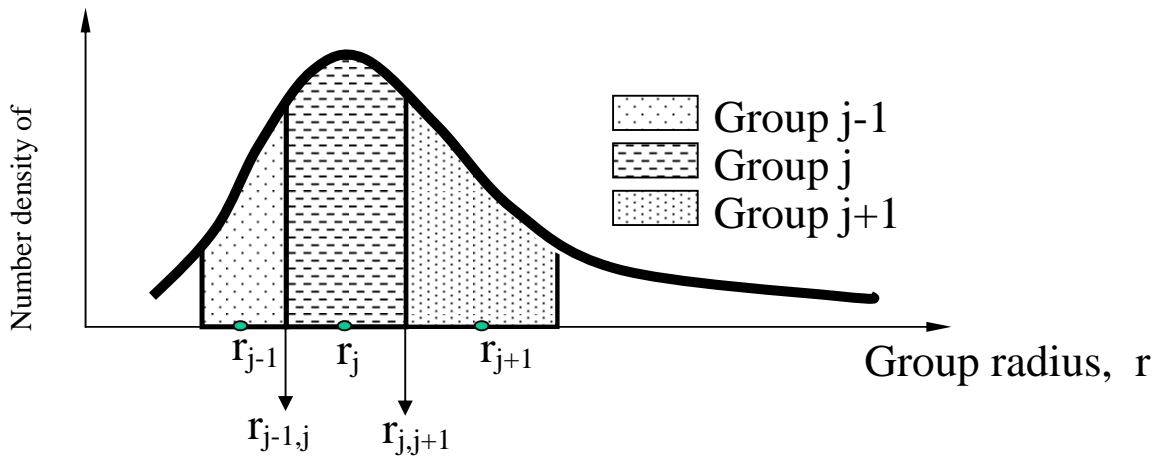
group are therefore

$$V_j = R_V^{j-1} V_1 \tag{4}$$

$$r_j = R_V^{(j-1)/3} r_1 \tag{5}$$

where r_1 is the radius of a pseudo-molecule. According to Mukai et al, $V_m=3.433\times10^{-5}$ m^3/mol, so $r_1=2.39\times10^{-10}$ m. [32]

The critical radius that separates groups j-1 and j is $r_{j-1,j}$, which is the mean value of r_{j-1} and r_j, i.e.,

$$r_{j-1,j} = \frac{r_{j-1} + r_j}{2} = \frac{1}{2}\left(R_V^{\frac{j-2}{3}} + R_V^{\frac{j-1}{3}} \right) r_1 \tag{6}$$

$$V_{j-1,j} = \left[\frac{1}{2}\left(R_V^{\frac{j-2}{3}} + R_V^{\frac{j-1}{3}} \right) \right]^3 V_1 \tag{7}$$
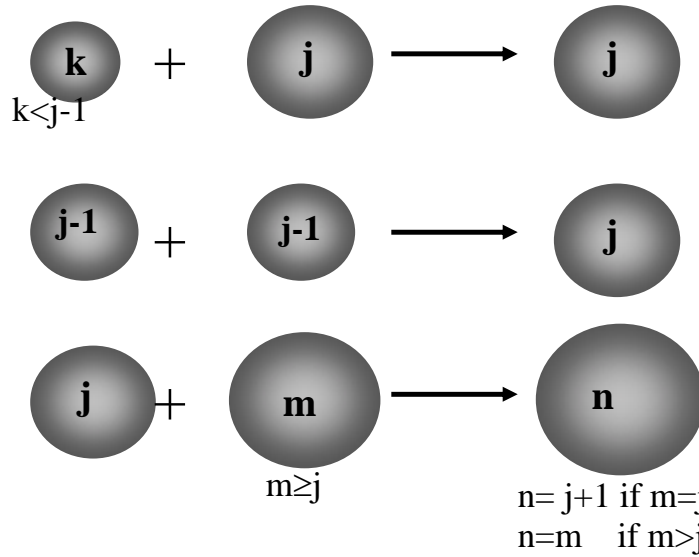

Fig.3 Schematic of inclusion population balance for the group j

For the inclusions in group j, only the following collisions are related to its population balance:

4

1. Inclusion j collides with inclusion j-1 or smaller, generating new inclusions still in group j, but with larger volume;
2. Inclusion j-1 collides with inclusion j-1, generating new j inclusions, but with smaller volume;
3. Inclusion j collides with inclusions larger than j-1, generating new inclusions larger than j (and thereby decreasing the number of inclusions in group j)

As an example, we let j=10, then $V_{j-1,j}$=2498V_1, $V_{j-1}+V_{j-1}$=3052V1,V_j=3814V_1, V_j+V_{j-1}=5340V_1, $V_{j,j+1}$=6246V_1, V_{j+1}=9536V_1. Therefore, size j-1 colliding with j-1 generates new inclusions in group j; j colliding j-1 generates new inclusions still in group j. This finding holds for at least 2.1≤R_V≤2.9.

The relationship between group k, the number of Al_2O_3 molecules it contains, and its radius are summarized in **Table I**. Thus, performing a calculation for 50 groups should be enough to span the complete size range of inclusions found in molten steel.

Table I The group number and its radius in size group model

Group No. (k)	Monomers contained	r_k (μm)
1	2.5^0=1	2.39×10^{-4}
2	2.5^1=2.5	3.24×10^{-4}
3	2.5^2=6.25	4.40×10^{-4}
10	2.5^9=3.8$\times10^3$	3.73×10^{-3}
20	2.5^{19}=3.6$\times10^7$	7.91×10^{-2}
30	2.5^{29}=3.5$\times10^{11}$	1.68
40	2.5^{39}=3.3$\times10^{15}$	35.61
50	2.5^{49}=3.2$\times10^{19}$	755.24

Considering the critical size group j_c for a stable particle, the evolution equations become:
① $2 \le j < j_C$ (namely nucleation)

$$\frac{dN_j}{dt} = N_j \beta_j^D N_1 \frac{V_1}{V_j} - \alpha_j A_j N_j \frac{V_1}{V_j} \tag{8}$$

② $j \ge j_C$ (namely growth)

$$\frac{dN_j}{dt} = N_j \sum_{k=1}^{j-1} \left(\phi_{kj} \left(\beta_{kj}^T + \beta_{kj}^B \right) N_k \frac{V_k}{V_j} \right) + \phi_{j-1,j-1} \left(\beta_{j-1,j-1}^T + \beta_{j-1,j-1}^B \right) N_{j-1} N_{j-1} \frac{2V_{j-1}}{V_j}$$

$$- \sum_{k=j}^{j_{max}-1} \left(1 + \delta_{jk} \right) \phi_{jk} \left(\beta_{kj}^T + \beta_{kj}^B \right) N_j N_k \tag{9}$$

$$+ N_j \beta_i^D N_1 \frac{V_1}{V_k} - \alpha_j A_j N_j \frac{V_1}{V_j}$$

The rate constant for pseudo-molecule diffusion, β_i^D, is expressed by [31]

$$\beta_i^D = 4\pi D_1 r_i. \tag{10}$$

Particle collisions are governed by the following rate constants

$$\beta_{ij}^B = \frac{2kT}{3\mu} \left(1/r_i + 1/r_j \right) \left(r_i + r_j \right), \tag{11}$$

$$\beta_{ij}^T = 1.3 \left(r_i + r_j \right)^3 \left(\varepsilon/v \right)^{1/2} \tag{12}$$

where β_{ij}^B represents Brownian collision [33] and β_{ij}^T represents turbulent collision, based on Saffman's model [34]. The coagulation constant, φ, is a probability function based on the Hamaker constant, inclusion size, etc. [29], but is assumed here to equal 1 for this simple nucleation model.

Ostwald-ripening involves both growth (from diffusion governed by $\beta_{D,i}$ and dissociation, which is governed by the dissociation rate constant α_i. This dissociation rate constant is found by tracking the diffusion of pseudo-molecules, $\beta_{D,i}$. Unstable particles, $(i<i_c)$ can grow or shrink only due to diffusion, while stable inclusion particles, $(i>i_c$ and $r>r_c)$ evolve according to both diffusion and collision. According to Kampmann [31], the relationship between molecule dissolution rate α $(m^{-2}s^{-1})$ and the rate constant for pseudo-molecule diffusion can be shown as

$$\alpha_i A_i = \beta_{1i} N_1 \tag{13}$$

The Gibbs-Thomson equation reads in the present notation [35]

$$\frac{N_1}{N_{1,eq}} = \exp\left(\frac{2\sigma V_m}{RT}\frac{1}{r_i}\right) = \exp\left(\frac{2\sigma V_m}{RT}\frac{1}{r_1\left(R_V^{i-1}\right)^{1/3}}\right). \tag{14}$$

Thus

$$\alpha_i A_i = \beta_i^D N_1 = \beta_i^D N_{1,eq} \exp\left(B \cdot R_V^{\frac{1-i}{3}}\right) \tag{15}$$

If fractal theory is included in the model to consider the effect of alumina cluster morphology, the radius of an alumina cluster can be given by [36]

$$r_i^{Cluster} = M^{1/D_f} r_1, \tag{16}$$

where M is the number of separate particles in the cluster — alumina molecules for the current model which includes nucleation. For the current study, $M = R_V^{i-1}$, which yields

$$r_i^{Cluster} = R_V^{\frac{i-1}{D_f}} r_1, \tag{17}$$

where D_f is the fractal dimension. The value of D_f is 1.3-1.8 [37] for microstructural features observed in two dimensions, but is actually 2.0-2.5 [38] for three dimensional observations. D_f is assumed to be 3 in this work, and in this work r_j refers to the equivalent radius sphere, so that its density is that of alumina. The effect of the radius and density of alumina clusters has been studied by Miki and Thomas [36], and will be investigated in further study in this project.

Dimensionless versions of Eq.(8) and (9) can be obtained by making the following substitutions:

$$\left.\begin{array}{l} N_i^* = \dfrac{N_i}{N_{1,eq}} \\[3mm] t^* = t \Big/ \left(\dfrac{1}{\beta_1^D \cdot N_{1,eq}}\right) \\[3mm] \beta_i^{D^*} = \beta_i^D / \beta_1^D \\[2mm] \beta_{ij}^{B^*} = \beta_{ij}^B / \beta_1^D \\[2mm] \beta_{ij}^{T^*} = \beta_{ij}^T / \beta_1^D \\[2mm] \alpha_i^* = \alpha_i \Big/ \left(\dfrac{\beta_1^D \cdot N_{1,eq}}{A_i}\right) \end{array}\right\} \tag{18}$$

According to classical homogenous nucleation theory, the critical radius of nucleus r_C is [12]

$$r_C \equiv \frac{2\sigma V_m}{RT \ln \Pi}. \tag{19}$$

If $r > r_C$, nucleation occurs, and stable particles precipitate and start to grow. According to Eq.(19),

6

the critical size of nucleus decreases with increasing supersaturaion Π and decreasing surface tension.

If j_c is the critical group number, beyond which nucleation occurs, the number of molecules in j_c inclusions is:

$$\frac{V_{jc}}{V_1} = \frac{R_v^{jc-1}V_1}{V_1} = R_V^{jc-1}. \tag{20}$$

On the other hand, Eq.(19) also yields that the number of molecules in j_c inclusions is:

$$\left(\frac{r_C}{r_1}\right)^3 = \left(\frac{2\sigma V_m}{RTr_1}\frac{1}{\ln\Pi}\right)^3. \tag{21}$$

Eq.(20) should equal to Eq.(21), which gives

$$j_c = 1 + \frac{3}{\ln R_v}\ln\left(\frac{2\sigma V_m}{RTr_1}\frac{1}{\ln\Pi}\right) \tag{22}$$

For alumina inclusions, σ=0.5N/m, R_v=0.5, and Π=40 yield $2\sigma V_m/(RTr_1)$=9.22 and j_c=4, which means that the critical size for nucleation is in group 4, including R_v^{4-1}=64 alumina molecules.

The supersaturation of free Al_2O_3 molecules, Π, in Eq.(19) is represented by

$$\Pi \equiv \frac{N_1}{N_{1,eq}}, \tag{23}$$

where $N_{1,eq}$=2.634×10^{23} m^{-3} corresponds to 3ppm dissolved oxygen in steel at equilibrium. According to a mass balance, the supersaturation can be expressed by

$$\Pi = \frac{N_S(t)}{N_{1,eq}} - \sum_{i=2}^{\infty}\frac{N_i}{N_{1,eq}} \cdot R_v^{i=1}. \tag{24}$$

where N_S is the total number of Al_2O_3 molecules including those in nucleated inclusions, which is a function of dimensionless time, represented by Eq.(25) [31], which defines how fast the Al_2O_3 molecules appear and disperse in the liquid steel after the deoxidizer-Al is added.

$$N_S^*(t^*) = N_{s,eq}^*\left[1.0 - \exp(-\frac{t^*}{\tau})\right], \tag{25}$$

where $N_{S,eq}$ is the equilibrium total number of Al_2O_3 molecules that form in the liquid steel, corresponding to the initial oxygen content before deoxidation.
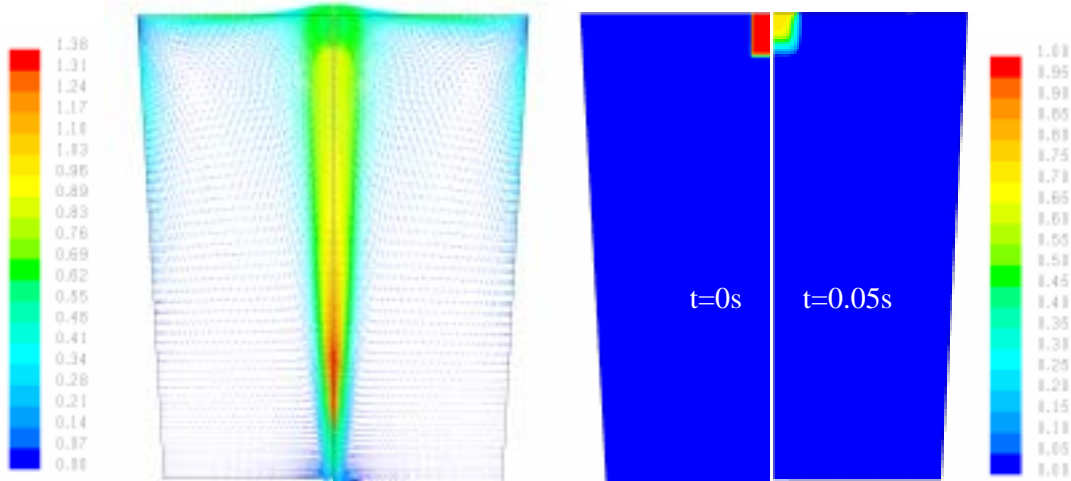

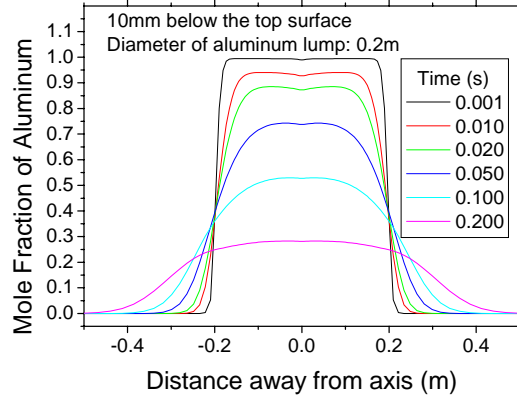Fig.4 Fluid flow and aluminum dissolution in a 300-tonne argon-stirred steel ladle

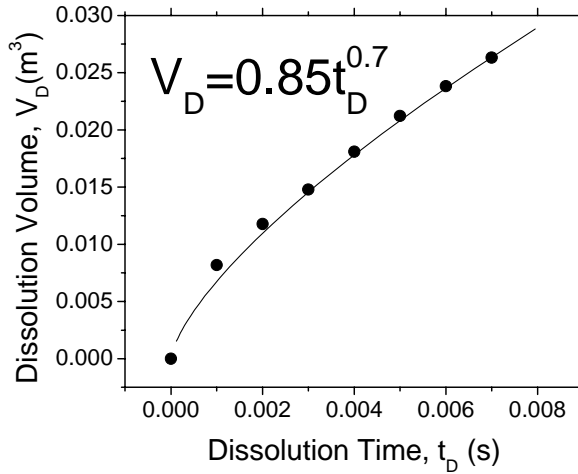Fig. 5 The dissolution and transport of aluminum near the first adding place

Fig. 6 The dissolved volume of aluminum as a function of time

A rate constant τ is introduced to account for the time needed for a lump of aluminum alloy added to the ladle to dissolve into aluminum atoms, ie., the initial pseudo-molecular alumina concentration, due to reaction and diffusion of the deoxidant. The value of τ should depend on the diffusion of aluminum in molten steel and the flow condition. For a 300tonne argon stirred ladle (argon flow rate is 0.5 Nm^3/min, ladle height is 4.5m), the fluid flow pattern, the motion and dissolution of a aluminum lump is shown in **figure 4**. **Figure 5** shows that the aluminum mole fraction distribution near the surface of the aluminum lump increases rapidly as the lump dissolves into the surrounding molten steel. **Figure 6** shows that the volume of dissolved aluminum increases with time according t:

$$V_D = 0.85 \cdot t_D^{0.7} \tag{26}$$

Eqs.(8)-(9) are solved using the Runge-Kutta method. The following material properties are chosen to model steel deoxidation at 1823K: D_1=2.5$\times$10^{-9} m^2/s (diffusion coefficient of oxygen in liquid steel, $D_1 = 5.59 \times 10^{-7} \exp(-81900/8.314T)$) [39], ρ_L=7000 kg/m^3, ρ_p=2700 kg/m^3, μ_L=0.0067 kg.m^{-1}s^{-1}. The surface tension between Al$_2$O$_3$ particles and liquid steel is 0.5 N/m [40]. $N_{1,eq}$=2.634$\times$10^{23} m^{-3} corresponding to the 3ppm dissolved oxygen in steel. Therefore β_1^D=7.50$\times$10^{-18} m^3/s, and

$$t^* = 1.98 \times 10^6 t \tag{27}$$

Eq.(25) therefore can be rewritten into

$$\frac{N_{s,eq}^* - N_S^*(t^*)}{N_{s,eq}^*} = \exp\left(-\frac{t^*}{\tau}\right) \tag{28}$$

Now we assume

$$\frac{N_{s,eq}^* - N_S^*(t^*)}{N_{s,eq}^*} = 0.001, \tag{29}$$

Substituting Eq(26), (27), and (29) into Eq.(28) gives

$$\tau = 2.87 \times 10^5 t_D \tag{30}$$

RESULTS OF NUMERICAL SIMULATION

The model was applied to aluminum deoxidation of a typical steel-oxygen system, where measurements and calculations were available. The vessel was a 50 tonne ladle of low-carbon steel refined in an ASEA-SKF furnace.[41] The ladle had 2.3m diameter and 1.7m depth, which corresponds to a turbulent energy dissipation rate in the melt of 0.01224 m^2/s^3 (856.8 erg/cm^{3}s). The total oxygen before adding aluminum is around 300 ppm and the final free oxygen is about 3 ppm, which corresponds to a 46kg aluminum addition and gives $N_{S,eq}=100 \times N_{1,eq}$. Thus, $N_{s,eq}^*=100$. If the aluminum is spherical lumps with diameter of 0.11m, each lump is 5.2×10^{-4} m^3 in volume, so the dissolution time is 2.59×10^{-5} s (Eq.(26)), and the value of τ is around 10 (Eq.(30)). This value is also used by Kampmann et al [31]. The total number of alumina molecules including those in inclusions can be rewritten from Eq.(25) to

$$N_S^* = 100\left[1.0 - \exp\left(-\frac{t^*}{10}\right)\right]. \tag{31}$$

Control Mechanisms of Inclusion Growth at Different Inclusion Size Ranges

The following scales can be defined according to the comparison of the pseudo-molecules diffusion rate constant with the collision rate constants (**Fig. 7**):

• Brownian scale $l_B<1\mu$m: where the growth of inclusions with radii in this range is controlled by diffusion of pseudo-molecules and Brownian collision. The irregular thermal movement that characterizes Brownian collisions is independent of fluid flow, and is not directional. Thus the inclusions tend to grow in every direction, leading to a spherical product;
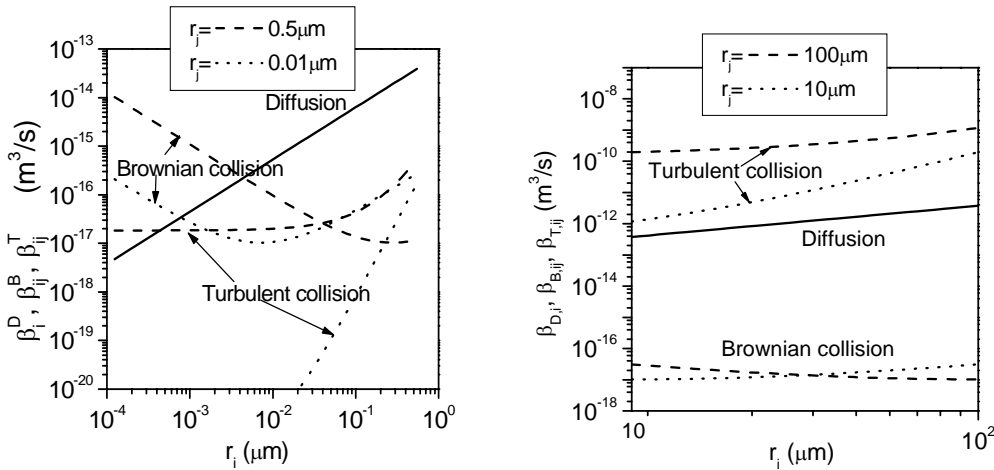

Fig. 7 Comparison of pseudo-molecule diffusion rate constant and collision rate constants

• Turbulent scale $l_T=2\sim l_e$, where l_e is the characteristic size of the smallest turbulence eddy, on the order of $l_e=(v^3/\varepsilon)^{1/4}$, and around 90µm for the current system. Inclusions with radii in this range grow by turbulent collisions, and the diffusion of pseudo-molecules is not as important, due to the low concentration of pseudo-molecules. Solid inclusions in this range tend to retain smallest features of 1~4µm in diameter as shown in Fig.2;

• Intermediate scale $l_I=l_B\sim l_T$, where the growth of inclusions in is controlled both by pseudo-molecules diffusion and by collisions (Brownian collision and turbulent collision);

Inclusion morphology is therefore summarized as follows: Fine inclusions grow spherically to 1 to 2 µm in radii due to diffusion and Brownian collision after nucleation. When there is a shortage of nuclei, single particles can grow into large dendritic structures due to unstable growth into high concentrations of diffusing pseudo-molecules. Otherwise, clusters of particles will form due to turbulent collisions resulting from flowing liquid steel. With time, the surface contours of all particles becomes progressively smoother due to the diffusion process called "Ostwald ripening".

Incubation, Nucleation and Growth of Inclusions

Figure 8 shows the supersaturation Π , the number of particles ζ and the critical size of nucleus i_c as a function of time. After aluminum addition, the aluminum and oxygen react to form pseudo-molecules. Groups of pseudo-molecules are generated from diffusion. With the further addition and dispersion of aluminum, the concentration of pseudo-molecules continues to increase. At time $t=t_2$, the radii of some groups of pseudo-molecules become equal to r_c, thus nucleation begins. Particles precipitate and start to grow. Thus the incubation period is $0\sim t_2$. Calculation indicates that the incubation period is very short, only 0.53µs. At $t=t_2$, the first particle appearing in the melt has $i_c=42$ ($r=8.3$ Å). Thus $i=42$ is the largest group of pseudo-molecules, all of those larger than this size nucleate and become particles. After time t_2, smaller inclusions can precipitate and grow by diffusion of pseudo-molecules, and collision with other inclusions. This starts a size distribution range. The supersaturation Π gradually increases from zero to its maximum (46.7) at time t^*_3 =8.07 (t_3=3.40µs). This
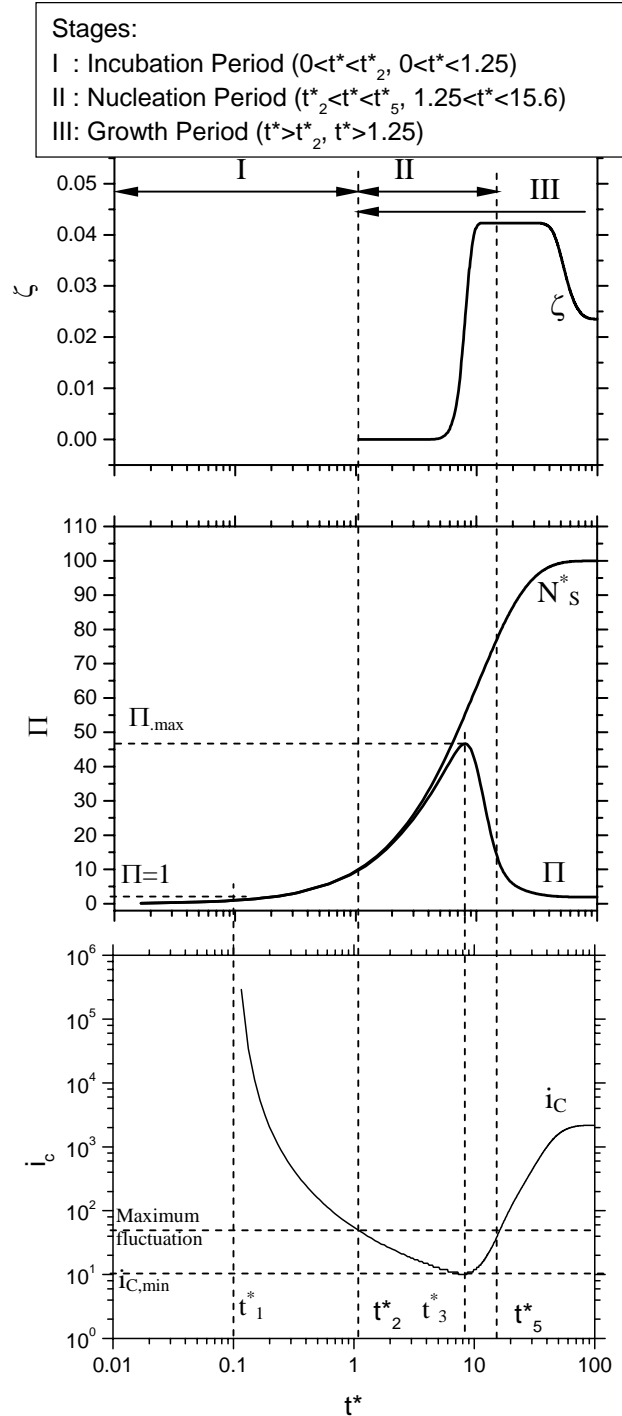
Stages:
I : Incubation Period ($0<t^*<t^*_2$, $0<t^*<1.25$)
II : Nucleation Period ($t^*_2<t^*<t^*_5$, $1.25<t^*<15.6$)
III: Growth Period ($t^*>t^*_2$, $t^*>1.25$)

Fig. 8 Calculated ζ, Π, i_c *versus* time

10

corresponds to the decrease in critical nucleus size to its smallest-sized stable nucleus (r_c =5.15Å, containing i=10 pseudo-molecules) at time t_3. Groups containing less than 10 pseudo-molecules are not stable particles. Nucleation is possible only during the time period $t^*_2 \sim t^*_5$ (0.53~6.58μs), when the critical nucleus size is smaller than the largest sized group of pseudo-molecules (forming by random diffusion).

Figure 9 shows a histogram of inclusion size distribution at different times, assuming that all inclusions with radii larger than 36μm are instantly removed to the top slag. With increasing time, this size distribution range becomes larger and larger, reaching 0.1~1μm at 6s and 0.1~36μm at 100s. When t=6s, the largest inclusion is around 2 μm diameter, which agrees roughly with the industrial measurements [42]. It takes about 100sec for the inclusions to grow to several tens of microns, which agrees well with the study of Kawawa et al [15].
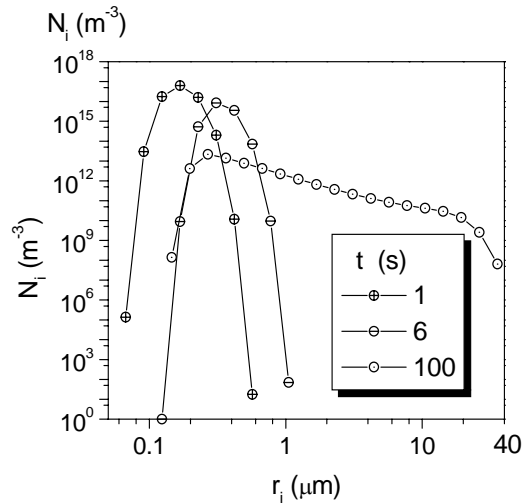
Figure 10 indicates that with increasing time, the number of smaller inclusions drops, and some new bigger inclusions are generated mainly by collision. The inclusion concentration changes with time: first

Fig. 9 Inclusion size distribution as a function of time

increasing to a maximum value and then slowly decreasing. The calculation indicates that after 720 seconds, the total oxygen concentration in the liquid steel decreases to around 20 ppm, which agrees well with Nakanishi's measurement (**figure 11**). [41]
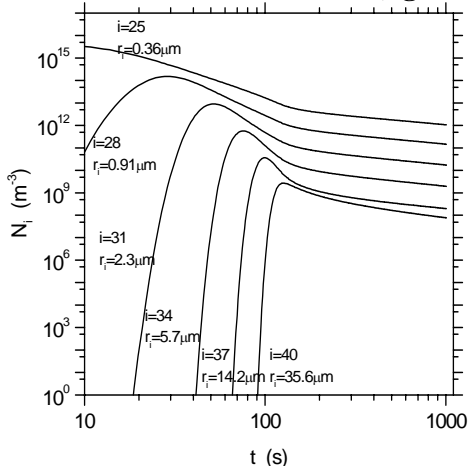

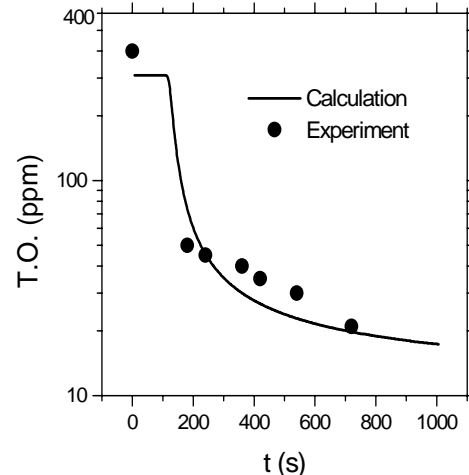**Fig.10** Inclusion concentration *versus* time

Fig.11 Comparison of total oxygen between calculation and experiment

Effect of Stirring Power on Inclusion Growth and Removal

Stirring power is an important parameter controlling the steel refining process. Favorable metallurgical reactions require strong mixing to bring the metal and slag into contact at their interface (e.g. desulphurisation, dephosphorisation, deoxidation, and inclusion removal), whereas other detrimental phenomena favor less mixing, such as maintenance of an unbroken slag layer, and avoiding erosion of the vessel refractories. The effect of stirring power on the oxygen removal rate constant is shown in **Fig. 12** [43, 44]. Excessively strong stirring is detrimental as the upward circulation of steel onto the slag layer may expose an "eye" region of the steel surface to reoxidation and the lining may be seriously eroded. **Table II** gives the specific stirring powers for different

refining process, based on analysis of literature data. Natural convection in the ladle and flow through the tundish produces the lowest mixing power, while vigorous stirring in NK-PERM vessels has the largest. Argon gas bubbling, DH, and steel tapping are intermediate. The SEN delivering steel into the mold has a similar stirring power to the most vigorous refining processes, although the time is very short.
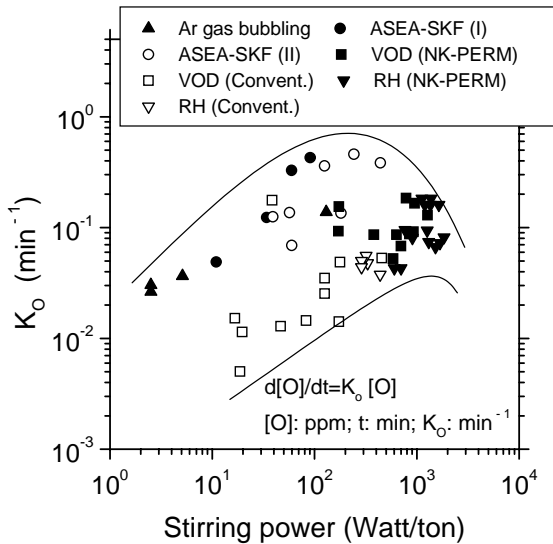

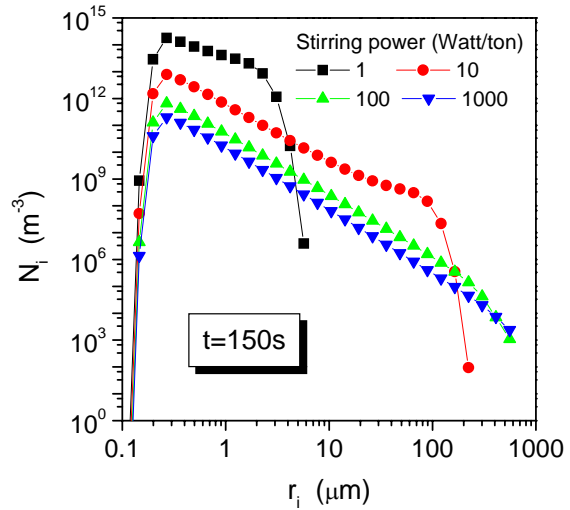**Fig. 12** Effect of stirring power on deoxidation rate constant

Fig. 13 Effect of stirring power on inclusion size distribution

Table II Stirring powers for different processes and regimes

Stirring pattern	Power (Watt/ton)
Argon gas bubbling [43, 45]	2-130 [43], 43-214 [45]
Tapping steel [45]	17-286
DH [45]	72-100
ASEA-SKF [43, 45, 46]	7-29 [45], 10-250 [43], 200-600 [46]
PM (Pulsation Mixing) [45]	10
RH [44, 45]	86-114 [45], 200-400 (conventional) [44], 500-3000 (NK-PERM) [44]
VOD [44]	10-400 (conventional), 100-800 (NK-PERM)
Outlet of SEN in continuous casting mold [46]	470-800
Tundish inlet zone [46]	10-50
60 ton ladle [46]	1-50

The calculated effect of stirring power on inclusion size distribution is shown in **Fig. 13**, which indicates that increasing stirring power generates more large inclusions in the bulk. If these inclusions can be removed into the slag, this improves cleanliness. This is very bad for steel cleanliness, however, if the stirring power is high at the end of refining, when the new large inclusions have no time to be removed. Therefore, the recommended practice is to first stir vigorously, to encourage the collision of small inclusions into large ones, followed by a "final stir" that slowly recirculates the steel to facilitate their removal into the slag while minimizing the generation of more large inclusions via collisions.

Ladle Mixing Times

When deciding the constant τ in Eq. (25), the aluminum dissolution is considered. Aluminum is added into molten steel from solid aluminum to melt and dissolve into free aluminum atoms. Once the solid aluminum is dissolved, the aluminum atoms are available to react with the free oxygen in the molten steel to generate alumina inclusions. The calculated nucleation time is in the order of $1\mu s$, which is very fast compared with the mixing of aluminum atoms in the molten steel. **Figure 14** shows the aluminum dispersion in an argon stirred ladle of molten steel continued from Fig.4, which indicates that the mixing process is much slower, roughly 10^8 slower than the nucleation process.
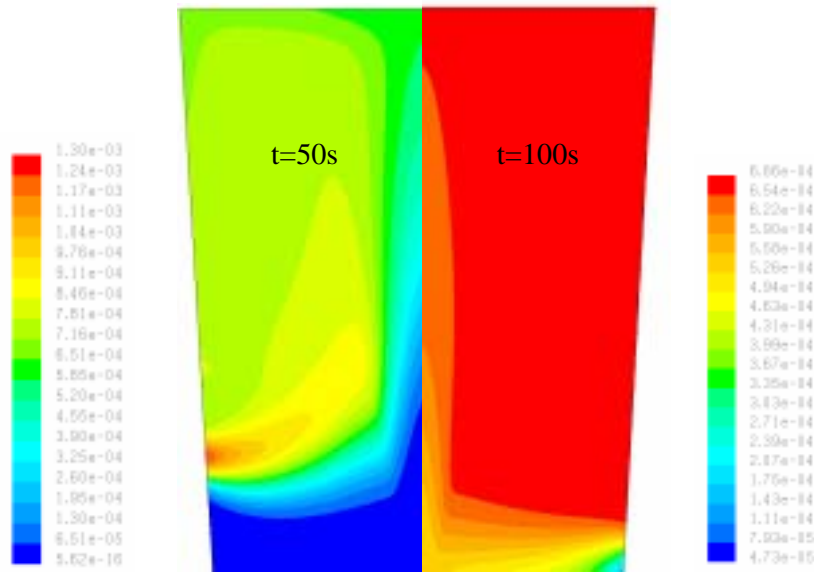

Fig.14 Aluminum mass fraction distribution in ladle at different time

The aluminum mass fraction changes with time at different points as shown in **figure 15**. The mixing time is defined as the time at which the mass fraction reaches 95% of the infinite average fraction. The calculated mixing times vary greatly at different points in the ladle, as shown in **figures 16 and 17**. Within this uncertainty, the computations in figure 17 agree with previous measurements. [47] Inclusion trajectories in this argon-stirred ladle also shown in Fig.16, which indicates a long moving path length before inclusions reach the top surface to be removed. Increasing stirring power naturally decreases the mixing time, as shown in figure 17.
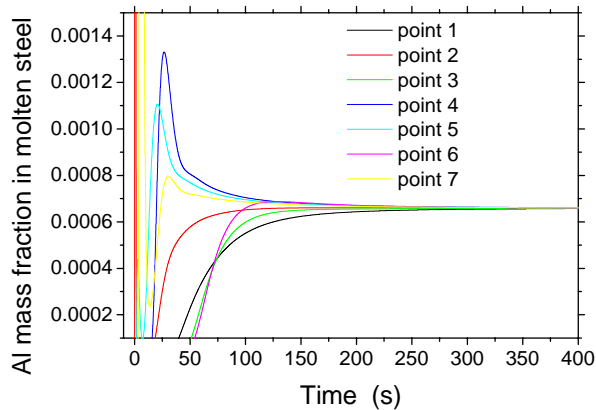

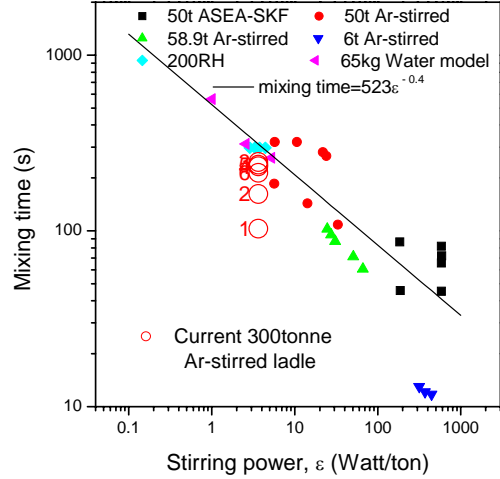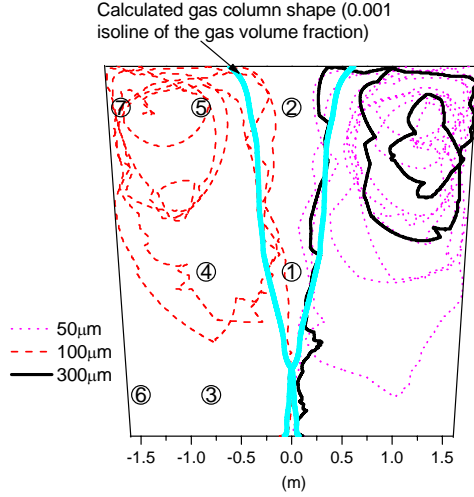Fig.15 Al dispersion in molten steel of a gas-stirred ladle

Fig.16 Inclusion trajectories in argon stirred ladle   Fig.17 Mixing time deceasing stirring power

FUTURE WORK

The mixing process and inclusion motion all should be included in the further investigation of inclusion nucleation, growth, transport, and removal. The nucleation and growth of inclusions should be coupled with fluid flow. Specifically, the following transport equations which include these phenomena should be solved:

$$\frac{\partial}{\partial t}\left(N_j\right)+\frac{\partial}{\partial x_i}\left[\left(u_i+V_{T,i}\right)N_j\right]-\frac{\partial}{\partial x_i}\left(D_{eff}\frac{\partial N_j}{\partial x_i}\right)=S_j \tag{32}$$

where N_j is the concentration of inclusions (with radius r_j) in number per m^3 of molten steel. V_T is the terminal rising velocity of inclusions. For small particles, Stokes flow can be assumed, so V_T is defined as follows (gravitational force is downward in z direction):

$$V_{T,i}=\left(0, \quad 0, \quad \frac{2\left(\rho-\rho_p\right)gr_i^2}{9\mu}\right) \tag{33}$$

The effective diffusion coefficient, D_{eff}, depends on the local effective viscosity, μ_{eff}, which is obtained by some turbulence model.

$$D_{eff}=D_1+\frac{\mu_{eff}}{\rho_p Sc_t} \tag{34}$$

where D_1 is the laminar (molecular) diffusivity, m^2/s; Sc_t is the turbulent Schmidt number.

The source term at RHS of Eq.(32) is represented by
① $2\leq j<j_C$ (namely nucleation)

$$S_j=N_j\beta_j^D N_1\frac{V_1}{V_j}-\alpha_j A_j N_j\frac{V_1}{V_j} \tag{35}$$

② $j\geq j_C$ (namely growth)

14

$$S_j = N_j \sum_{k=1}^{j-1} \left(\phi_{kj} \left(\beta_{kj}^T + \beta_{kj}^B \right) N_k \frac{V_k}{V_j} \right) + \phi_{j-1,j-1} \left(\beta_{j-1,j-1}^T + \beta_{j-1,j-1}^B \right) N_{j-1} N_{j-1} \frac{2V_{j-1}}{V_j}$$

$$- \sum_{k=j}^{j_{max}-1} \phi_{jk} \left(\beta_{kj}^T + \beta_{kj}^B \right) N_j N_k + N_j \beta_i^D N_1 \frac{V_1}{V_k} - \alpha_j A_j N_j \frac{V_1}{V_j}$$

(36)

Eqs. (35) and (36) are from Eqs.(8) and (9).

CONCLUSIONS

1. A computational model based on classic homogenous nucleation theory, thermodynamic analysis and population balance equations, has been developed to study steel deoxidation by aluminum in a low carbon aluminum-killed steel ladle. The model calculates the nucleation and time evolution of the alumina inclusion size distribution due to Ostwald ripening, Brownian collision and turbulent collision.

2. For the given conditions, the nucleation is very fast, occurring mainly between 1μs and 10μs. The stable inclusion nuclei are predicted to be only about 10-20 Å in diameter (containing on the order of 10-100 pseudo-molecules of alumina). After this time, the size distribution of the stable inclusion particles grows by the diffusion / dissolution of pseudo-molecules (Ostwald-Ripening) and by collisions. The inclusion size distribution reaches 0.1~1μm at 6s and 0.1~36μm at 100s. When t=6s, the largest inclusion is around 2 μm diameter.

3. The growth of inclusions smaller than 1μm, is mainly controlled by diffusion of pseudo-molecules and Brownian collision. Inclusions in this range tend to be spherical. The growth of inclusions larger than 2μm is mainly controlled by turbulent collisions. Inclusions in this range tend to form clusters which retain minimum feature sizes of 1~2μm.

4. Computations with this model of the inclusion size range in a ladle roughly agree with experimental measurements.

5. The inclusion size distribution evolves to form larger inclusions with increasing stirring power. Actual steel refining processes have a range of different stirring powers.

6. For optimal inclusion removal, it is recommended to first stir vigorously, to encourage the collision of small inclusions into large ones. This should be followed by a "final stir" that slowly recirculates the steel to facilitate their removal into the slag while minimizing the generation of more large inclusions via collisions.

7. Mixing simulations reveal that mixing requires several hundred seconds, depending on location in the ladle and stirring power. This is 8 orders of magnitude slower than nucleation phenomena.

8. Further studies should be coupled with fluid flow and include the effects of deoxidant composition (Si and Al), deoxidant flow transport, interfacial tension, diffusion coefficient, the initial oxygen content, and temperature on inclusion nucleation and growth. In addition, the phenomena of bubble-related collisions, cluster morphology, reoxidation, realistic inclusion transport and collision in the turbulent flowing liquid, and removal at the top slag layer and walls on inclusion evolution also need investigation before steel deoxidation and inclusion phenomena can be fully understood.

NOMENCLATURE

A_i The surface area of particle i, m^2

D_1 the diffusion coefficient of the pseudo-molecules in liquid , m^{2}s^{-1}

D_f Fractal dimension

i, j	The particle size, namely, this particle is comprised of i pseudo-molecules or j pseudo-molecules
i_c	the critical size for nucleus, m
k	The Boltzmann constant, $J.K^{-1}$
l_e	The size of the smallest eddy in turbulence flow, m
l_B, l_I, l_T	Brownian scale, Intermediate scale, and turbulence scale respectively, m
M	The number of separate particles in a cluster
N_A	The Avogadro number, mol^{-1}
N_1	The concentration of the dissolved pseudo-molecules, m^{-3}
$N_{1,eq}$	The concentration of the dissolved pseudo-molecules at equilibrium, m^{-3}
N_i	The average concentration of the particle i, m^{-3}
$N_S(t)$	The total number of molecules including those in particles in the molten steel, m^{-3}
$N_{S,eq}$	The total number of molecules including those in particles in the molten steel at the equilibrium state, m^{-3}
R	Gas constant, 8.314 $J.k^{-1}mol^{-1}$
R_v	The ratio of volume of inclusions in two neighboring groups
r	The particle radius, m
r_c	The critical radius for nucleation, m
$r_i^{Cluster}$	Radius of aluminum cluster, m
r_i	The radii of the particle i, m
r_1	the radius of the pseudo-molecule, m
T	The absolute temperature, K
t	Time, s
t_2	Time for the beginning of nucleation, s
t_3	Time at $\Pi = \Pi_{max}$, s
t_5	Time for the ending of nucleation period, s
t_D	Dissolution time of aluminum in molten steel, s
t^*	The dimensionless time
V_i	The typical volume of inclusions in group I, m^3
V_D	Dissolution volume of aluminum in molten steel, m^3
V_m	Molecular volume of alumina inclusions, m^3/mol
α_i	The number of pseudo-molecules which dissociate per unit time from unit area of a particle of class i, $m^{-2}s^{-1}$
β^D_i	The diffusion rate constant of the molecules $m^3 s^{-1}$
$\beta^B_{ij}, \beta^T_{ij}$	Brownian and turbulent collision rate constant, $m^3 s^{-1}$
δ_{ij}	The Kronecker's delta function ($\delta_{ij}=1$ for i=j, and ($\delta_{ij}=1$ for i≠j)
ε	The turbulent energy dissipation rate, m^2s^{-3}
Π	The supersaturation of the parents phase, or the dimensionless concentration of pseudo-molecules
μ	The viscosity of the liquid, $kg.m^{-1}s^{-1}$
ϕ_{ij}	The coagulation coefficient of inclusions i and j[29]
ρ_L	The density of liquid, $kg.m^{-3}$
ρ_p	The density of particles, $kg.m^{-3}$
σ	The interfacial tension between alumina and liquid steel, $N.m^{-1}$
τ	Dimensionless constant related to aluminum dissolution and diffusion
ζ	The total dimensionless number density of growing particles
ν	The viscosity of the liquid, m^2s^{-1}

Superscripts
*	Dimensionless value

ACKNOWLEDGEMENTS

REFERENCES

1. S. Chakraborty and W. Hill, "Reduction of Aluminum Slivers at Great Lakes No.2 CC," 77th Steelmaking Conf. Proc., ISS, Warrendale, PA, Vol. 77, 1994, 389-395.
2. S. Chakraborty and W. Hill, "Improvement in Steel Cleanliness at Great Lakes No.2 Continuous Caster," 78th Steelmaking Conf. Proc., ISS, Warrendale, PA, Vol. 78, 1995, 401-413.
3. F.L. Kemeny, "Tundish Nozzle Clogging - Measurement and Prevention," in McLean Symposium Proceedings, ISS, Warrendale, PA, 1998, 103-110.
4. B.G. Thomas and H. Bai, "Tundish Nozzle Clogging ?Application of Computational Models," 78th Steelmaking Conf. Proc., Iron and Steel Society, Warrendale, PA, 2001, 895-912.
5. M. Byrne, T.W. Fenicle and A.W. Cramb, "The Sources of Exogenous Inclusions in Continuous Cast, Aluminum-Killed Steels," ISS Trans., Vol. 10, 1989, 51-60.
6. E.S. Szekeres, "Review of Strand Casting Factors Affecting Steel Product Cleanliness," 4th International Conference on Clean Steel,, (Balatonszeplak, Hungary), The Institute of Materials, London, UK, 1992, 756-776.
7. L. Ferro, J. Petroni, D. Dalmaso, J. Madias, C. Cicutti, "Steel Cleanliness in Continuous Casting Slabs," Steelmaking Conference Proceeding, (Warrendale, PA), ISS, Vol. 79, 1996, 497-502.
8. L. Zhang, B.G. Thomas, X. Wang, K. Cai, "Evaluation and Control of Steel Cleanliness - Review," in 85Steelmaking Conference Proceedings, Vol. 85, ISS, Warrandale, PA, 2002, 431-452.
9. R.A. Rege, E.S. Szekeres and W.D. Forgeng, "Three-Dimensional View of Alumina Clusters in Aluminum-Killed Low-Carbon Steel," Met. Trans. AIME, Vol. 1 (9), 1970, 2652.
10. R. Rastogi and A.W. Cramb, "Inclusion Formation and Agglomeration in Aluminum-killed Steels," in 2001 Steelmaking Conference Proceedings, Vol. 84, ISS, Warrendale, (Baltimore, Maryland, USA), 2001, 789-829.
11. T.B. Braun, J.F. Elliott and M.C. Flemings, "The Clustering of Alumina Inclusions," Metal. Trans. B, Vol. 10B (6), 1979, 171-184.
12. E.T. Turkdogan, "Deoxidation of Steel," JISI, 1972, 21-36.
13. Y. Miyashita and K. Nishikawa, "Measurement of Size Distribution of Nonmetallic Inclusions in Steel," Trans. ISIJ, Vol. 8, 1968, 181-185.
14. S. Linder, "Hydrodynamics and Collisions of Small Particles in a Turbulence Metallic Melt with Special Reference to Deoxidation of Steel," Scand. J. Metallurgy, Vol. 3, 1974, 137-150.
15. T. Kawawa and M. Ohkubo, "A Kinetics on Deoxidation of Steel," Trans. ISIJ, Vol. 8, 1968, 203-219.
16. E.T. Turkdogan, "Nucleation, Growth, and Flotation of Oxide Inclusions in Liquid Steel," JISI, 1966, 914-919.

17. M. Suzuki, R. Yamaguchi, K. Murakami, M. Nakada, "Inclusion Particle Growth during Solidification of Stainless Steel," ISIJ Inter., Vol. 41 (3), 2001, 247-256.

18. U. Lindborg and K. Torssell, "A Collision Model for the Growth and Separation of Deoxidation Products," Trans. ASME, Vol. 242, 1968, 94-102.

19. K. Nogi, "Wetting Phenomena in Materials Processing," Tetsu-to-Hagane, Vol. 84 (1), 1998, 1-6.

20. K. Okohira, N. Sato and H. Mori, "Observation of Three-Dimensional Shapes of Inclusions in Low-Carbon Aluminum-Killed Steel by Scanning Electron Microscope," Trans. ISIJ, Vol. 14, 1974, 103-109.

21. M. Olette, "Institut de Recherches de La Siderurgie Francaise," Report, IRSIO, 1972.

22. K. Asano and T. Nakano, "Deoxidation of Molten Steel with Deoxidizer," Trans. ISIJ, Vol. 12, 1972, 343-349.

23. H. Ooi, T. Sekine and G. Kasai, "On the Mechanisms of Alunima Cluster Formation in Molten Iron," Trans. ISIJ, Vol. 15, 1975, 371-379.

24. N. Aritomi and K. Gunji, "Morphology and Formation Mechanism of Dendritic Inclusions in Iron and Iron-Nickel Alloys Deoxidized with Silicon and Solidified Unidirectionally," Trans. ISIJ, Vol. 19, 1979, 152-161.

25. N. Aritomi and K. Gunji, "On the Formation of Dendritic Inclusion from a Spherical Primary Silica in Iron-10% Nickel Alloy Deoxidized with Silicon," Trans. ISIJ, Vol. 20, 1980, 26-32.

26. Y. Miki, H. Kitaoka, T. Sakuraya, T. Fujii, "Mechanism for Separating Inclusions from Molten Steel Stirred with a Rotating Electro-Magnetic Field," ISIJ Inter., Vol. 32 (1), 1992, 142-149.

27. W.K. Tiekink, A. Pieters and J. Hekkema, "Al2O3 in Steel: Morphology Dependent on Treatment," I & Smaker, Vol. 21 (7), 1994, 39-41.

28. T. Murai, H. Matsuno, E. Sakurai, H. Kawashima, "Separation Mechanism of Inclusion from Molten Steel during RH Treatment," Tetsu-to-Hagane, Vol. 84 (1), 1998, 13-18.

29. L. Zhang and S. Taniguchi, "Fluid Flow and Inclusion Removal in Continuous Casting Tundish," Metal. & Material Trans. B., Vol. 31B (2), 2000, 253-266.

30. J. Miyake and M.E. Fine, "Electrical Resistivity and the Gibbs-Thomson Equations," Scripta Metallurgica et Materialia, Vol. 25, 1991, 191-194.

31. L. Kampmann and M. Kahlweit, "On the Theory of Precipitations II," Berichte der Bunsen-Gesellschaft physikalische Chemie, Vol. 74 (5), 1970, 456-462.

32. K. Mukai, H. Sakao and K. Sano, "Non-metallic Inclusions Formed by Deoxidation Reaction in the Deoxidation Process- Deoxidation Reaction Zone," Trans. ISIJ, Vol. 9, 1969, 196-203.

33. S. Taniguchi and A. Kikuchi, "Mechanisms of Collision and Coagulation between Fine Particles in Fluid," Tetsu-to-Hagane, Vol. 78 (4), 1992, 527-535.

34. P.G. Saffman and J. S. Turner, "On the Collision of Drops in Turbulent Clouds," J. Fluid Mech., Vol. 1, 1956, 16-30.

35. J.M. B. Krishnamachari, B. Cooper, J. Stehna, "Gibbs-Thomson Formula for Small Island Sizes: Corrections for High Vapor Densities," Physical Review B, Vol. 54 (12), 1996, 8899-8907.

36. Y. Miki and B.G. Thomas, "Modeling of Inclusion Removal in a Tundish," Metall. Mater. Trans. B, Vol. 30B (4), 1999, 639-654.

37. J.L. LaRosa and J.D. Cawley, "Fractal Dimension of Alumina Aggregates Grown in Two Dimensions," J. Am. Ceram. Soc., Vol. 75 (1), 1992, 1981-1984.

38. D. Romeu, A. Gomez, J.G.Perez-Ramirez, R. Silva, O.L. Peres, A.E. Gonzalez, M. Jose-Yacaman, "Surface Fractal of Small Metallic Particles," Physical Review Letters, Vol. 57 (20), 1986, 2552-2556.

39. K. Mori and K. Suzuki, "Diffusion of Oxygen in Liquid Iron," Trans. ISIJ, Vol. 12, 1972, 464-471.

40. K. Wasai and K. Mukai, "Thermodynamics of Nucleation and Supersaturation for the Aluminum-Deoxidation Reaction in Liquid Iron," Metal. & Material Trans. B., Vol. 30B (6), 1999, 1065-1074.

41. K. Nakanishi and J. Szekely, "Deoxidation Kinetics in a Turbulent Flow Field," Trans. ISIJ, Vol. 15, 1975, 522-530.

42. F. Oeters, Metallurgy of Steelmaking, Verlag Stahleisen mbH, 1994, 347.

43. K. Ogawa, "Slag Refining for Production of Clean Steel," in Nishiyama Memorial Seminar, Vol. 143/144, Iron and Steel Institute of Japan, (ISS, Tokyo), 1992, 137-166.

44. M. Matsuno, Y. Kikuchi, M. Komatsu, M. Arai, K. Watanabe, H. Nakashima, "Development of New Deoxidation Technique for RH Degassers," I & Smaker, Vol. 20 (7), 1993, 35-38.

45. K.W. Lange, "Thermodynamic and Kinetic Aspects of Secondary Steelmaking Processes," Inter. Materials Reviews, Vol. 33 (2), 1988, 53-89.

46. L. Zhang and S. Taniguchi, "Fundamentals of Inclusions Removal from Liquid Steel by Bubbles Flotation," International Materials Reviews, Vol. 45 (2), 2000, 59-82.

47. J. Szekely, C.W. Chang and T. Lehner, "Flow Phenomena, Mixing and Mass Transfer in Argon-Stirred Ladles," Ironmaking & Steelmakaing, Vol. 6, 1979, 285.